# A Note on the Influence of Axial Velocity Ratio on Cascade Performance[1]

M. B. WILSON

*California Institute of Technology*

R. MANI

*University of Massachusetts*

A. J. ACOSTA

*California Institute of Technology*

A thin airfoil quasi-two-dimensional potential flow theory has been used to analyze cascades with axial-flow contraction. Attention is centered on the flow turning of a lattice of foils as measured by the deviation angle. The influence of both axial-flow acceleration and foil thickness on the deviation angle is summarized in plots that should be useful for design purposes. It is shown that the effect of axial-flow contraction is larger when the foils are relatively far apart than when they are close together. The influence of axial velocity ratio across the cascade changes markedly with the stagger angle. These effects are essentially unaltered due to foil thickness.

Design of axial-flow compressors and fans relies heavily on experimental data and simplified empirical rules (see, for example, ref. 1). Concurrent with experimental research, there have been strong advances in theoretical two-dimensional potential flow solutions of cascades (e.g., ref. 2). Within the limitation of assumed two-dimensionality, these theoretical solutions should be very useful in the interpretation and correlation of test data for

[1] All graphs, tables, equations and conclusions presented in this revised paper have been corrected from the earlier version presented at the symposium. The work providing the basis for this paper was carried out under Department of the Navy Contract Nonr 220(59).

design purposes. In an actual turbomachine design, of course, there is always a three-dimensional character to the flow, and one of the interesting consequences of this complication is that there is a change in the axial-flow velocity through the cascade. Recent theoretical calculations by Mani (ref. 3) contribute to the possibility of more rationally predicting the potential flow performance of a lattice of airfoils under conditions of a varying axial velocity. A survey of Mani's work appears in reference 4; reference 5 describes the computer techniques used in obtaining numerical results.

The purpose of this note is to outline some further results of computations using Quasi-two-dimensional theory (QTD) and to present these numerical data in the form of graphs and tables useful for design. Primary emphasis is placed on the influence of axial velocity ratio ($\mathrm{AVR} = Va_2/Va_1$) on cascade performance although, as will be seen later, wide ranges of most of the other cascade variables have been considered. In addition, we include some comparisons between existing theoretical results for two-dimensional cascade flows and the present results. The curves presented in the main body of this note are supplemented by the tables of data given in the appendix.

## THE QUASI-TWO-DIMENSIONAL CASCADE

The problem under consideration is that of the irrotational incompressible flow through an infinite cascade of airfoils spanning a channel whose width $h(x_1)$ changes slightly along the extent of the blade (figs. 1 and 2). Because $h(x_1)$ is a slowly varying function of $x_1$ only, the flow is very nearly two-dimensional (hence the term "quasi-two-dimensional"). In the study of plane cascades, the basic flow disturbed by the airfoils is represented by the vector mean $V_m$ of the inlet and outlet flow velocities. In the case of varying axial velocity, for reasons explained in the discussion of this paper, if $Va_1$ and $Va_2$ denote the axial velocities at the cascade leading and trailing edges and $Vt_1$ and $Vt_2$ the corresponding tangential velocities, the mean velocity representing the basic flow through the cascade (fig. 3) has an axial component $\frac{1}{2}(Va_1+Va_2)$ and a tangential component $V_{t_2}+\frac{1}{2}\Delta V_t(1+\alpha/2E)$, where $\Delta V_t = V_{t_1}-V_{t_2}$ and $\alpha$ and $E$ are contraction parameters shown later in figure 4.

### Cascade and Flow Parameters

Performance of a cascade system is usually represented by the amount of flow turning exerted by any one blade $\Delta\beta = \beta_1 - \beta_2$ as a function of all the remaining cascade and flow parameters. To some extent, performance is also indicated by the resulting circulation $\Gamma$ about an airfoil. In strictly

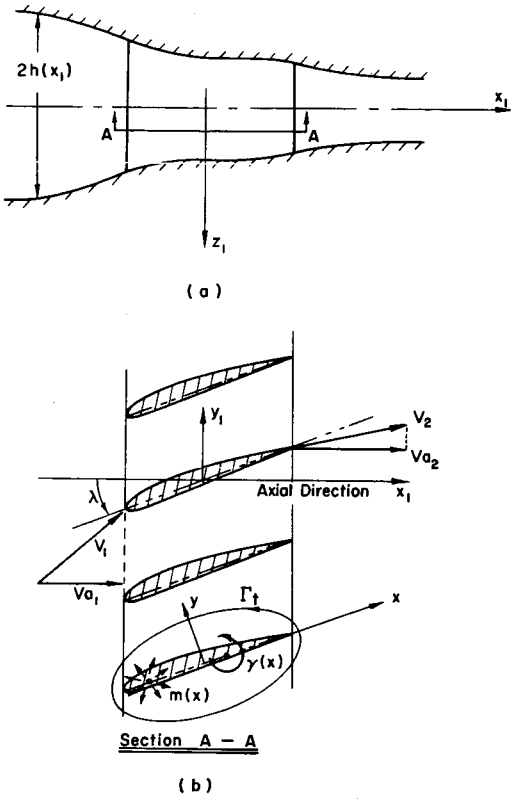


FIGURE 1.—*Schematic of flow through an infinite cascade of airfoils spanning a channel of varying width. Total circulation* $\Gamma_t$ *is measured positive counterclockwise (eq. (19)). In plane flow the foil nondimensional lift coefficient is* $C_L = -\Gamma_t = \Gamma$.

plane flow, the circulation is a direct measure of the lift exerted on the blade.

Figure 2 defines the various parameters of cascade and flow geometry. The notation adopted here differs slightly from that used by Mani in references 3, 4, and 5; it coincides more with Lieblein (ref. 1) and Mellor (ref. 2). In figure 2 all angles are indicated in their positive sense.

The inlet and outlet flow angles are

$$\left.\begin{aligned}\beta_1 &= \lambda + \frac{\theta_1}{2} + i \\ \beta_2 &= \lambda - \frac{\theta_2}{2} + \delta^*\end{aligned}\right\} \tag{1}$$

and the angle $\Delta\beta$ through which the flow is turned is

$$\Delta\beta = \tfrac{1}{2}(\theta_1 + \theta_2) + i - \delta^* \tag{2}$$

In the work to follow, the camber line is symmetric so that $\theta_1 = \theta_2$.

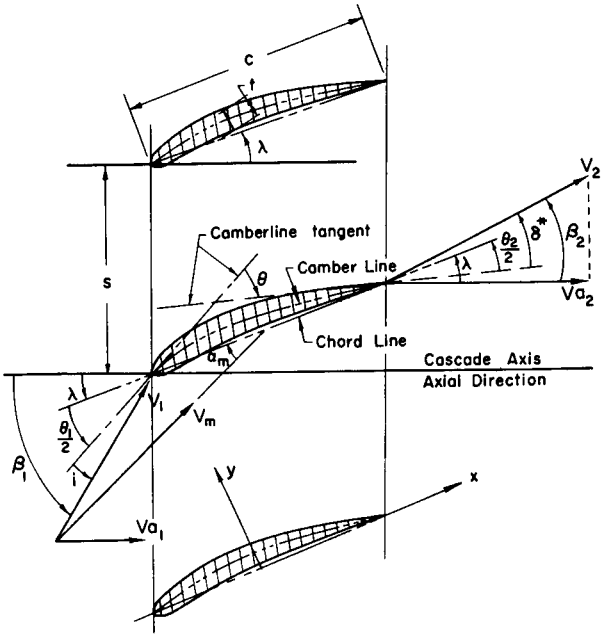


FIGURE 2.—*Definition sketch for the cascade and flow parameters.*

## Basic Equations

The quasi-two-dimensional (QTD) flow analysis is modeled after the approach and method of solution for plane flow cascades described in reference 2. There are several notable features of this theory that can be briefly mentioned here. The principal feature is that the governing equation of the strictly three-dimensional flow is reduced to a two-dimensional equation. This simplification can be made only because it is assumed that the channel width $h(x_1)$ is a slowly varying function. Beyond this, for simplicity, a channel contraction shape is adopted which minimizes the requisite calculations yet retains the essential features of the problem. In the present work there is the additional (but not essential) simplification that the thin airfoil approximations can be used. These same approximations have, in fact, been used before for plane cascade flow analysis with good effect (ref. 2) and are believed to be equally useful in the present case.

The key notion in this work is that all relevant quantities can be averaged over the channel height and that any errors that result are much smaller than the effect being sought. This idea is well known, as is indicated in reference 4, and rough estimates of the error involved can even be made (ref. 3). The flow is assumed to be an incompressible, potential

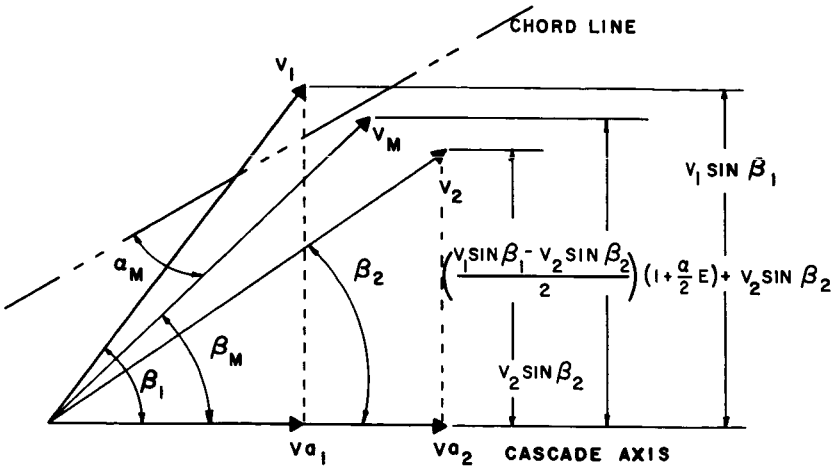


FIGURE 3.—*Velocity vector diagram.*

flow. There will be, accordingly, a velocity potential $\varphi(x,y,z)$ having velocity components $u(x,y,z) = \partial\varphi/\partial x$, etc. We define the following averages

$$\left.\begin{aligned} \bar{\varphi}(x_1,y_1) &= \frac{1}{h(x_1)} \int_0^h \varphi(x_1,y_1,z_1)\, dz_1 \\ \bar{u}(x_1,y_1) &= \frac{1}{h(x_1)} \int_0^h u(x_1,y_1,z_1)\, dz_1, \text{ etc.} \end{aligned}\right\} \tag{3}$$

It may then be shown (ref. 4) that

$$\left.\begin{aligned} \bar{u} &= \frac{\partial \bar{\varphi}}{\partial x_1} \\ \bar{v} &= \frac{\partial \bar{\varphi}}{\partial y_1} \end{aligned}\right\} \tag{4}$$

and that a quasi-two-dimensional stream function $\bar{\psi}(x_1,y_1)$ can be defined by

$$h\bar{u} = \frac{\partial \bar{\psi}}{\partial y_1}$$

$$-h\bar{v} = \frac{\partial \bar{\psi}}{\partial x_1}$$

In terms of the averaged flow quantities, the full three-dimensional flow field equations become

$$\left.\begin{aligned} \Delta\bar{\varphi}+\frac{h'(x_1)}{h(x_1)}\frac{\partial\bar{\varphi}}{\partial x_1}=0 \\ \Delta\bar{\psi}-\frac{h'(x_1)}{h(x_1)}\frac{\partial\bar{\psi}}{\partial x_1}=0 \end{aligned}\right\} \tag{5}$$

where $h'(x_1)\equiv dh/dx_1$. Fundamental solutions of these equations corresponding to source and vortex flows are clearly dependent on the channel shape through the function $h'(x_1)/h(x_1)$. The principal feature of the quasi-two-dimensional flow theory developed in reference 3 is that it takes explicit account of the fact that the velocity fields of sources and vortices should be calculated on the basis that these singularities themselves are modified by the lack of two-dimensionality.

Even from the equations quoted above for the average potential $\bar{\varphi}$ and stream function $\bar{\psi}$, it is clear that a good choice for the channel shape $h(x_1)$ is one for which the function $h'(x_1)/h(x_1)$ is as simple as possible. For this ratio equal to a constant, $-\alpha$ (a contraction), the result is an exponential channel shape $h(x_1)=h_0\exp(-\alpha x_1)$. A more realistic choice is one which gives a contraction effect and also constant stream velocities far upstream and far downstream. For purposes of the calculations in this report, a channel shape is chosen with a central contraction

$$\frac{h'(x_1)}{h(x_1)}=-\alpha[H_0(x_1+a)-H_0(x_1-a)] \tag{6}$$

where $H_0(x_1)$ is the Heaviside unit step function. This channel is sketched in figure 4*a* and can be conveniently termed a finite exponential channel.

Calculations of the fundamental source-like and vortex-like singularities of equation (5), even for the case of a finite exponential channel, are very complicated. It is only for the case of small contraction parameter $\alpha$ that the velocity components used for these computations can be approximated to the first order in $\alpha$; i.e., that the $x_1$-component of a unit vortex in axially accelerated flow can be expressed in the form

$$u_{\text{vortex}}=-\frac{1}{2\pi}\frac{y_1}{(x_1^2+y_1^2)}+\alpha u_{v_1} \tag{7}$$

where $u_{v_1}$ is a correction term for the non-two-dimensional character of the flow. Details of the calculations of all the necessary velocity components are contained in reference 3 and are summarized in reference 4. They all have the same form as equation (7), where the resulting formulas

are linear in $\alpha$. This points to a feature of the final results of the computations described in this note: they can be extended by linear extrapolation to any arbitrary but small $\alpha$.

The problem is nondimensionalized by putting the chord length $c=2$. The extent of the contraction ($2a$ in fig. 4$a$) is denoted by $E$. In the computer computations it is necessary to keep the ratio $E/2\cos\lambda>1.0$. Figure 4$b$ indicates the nondimensional channel geometry in the $x_1-z_1$ plane.

The axial velocity ratio is computed using the axial velocity components $Va_1$ and $Va_2$, measured at the leading edge and trailing edge, respectively. From the continuity equation, we have

$$\text{AVR}=\frac{Va_2}{Va_1}=\frac{h_0e^{\alpha\cos\lambda}}{h_0e^{-\alpha\cos\lambda}}=e^{2\alpha\cos\lambda} \tag{8}$$

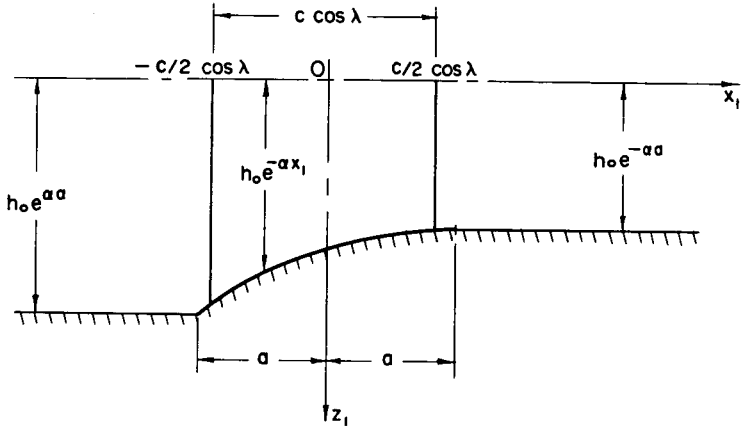


FIGURE 4$a$.—*Channel shape for a central contraction.*

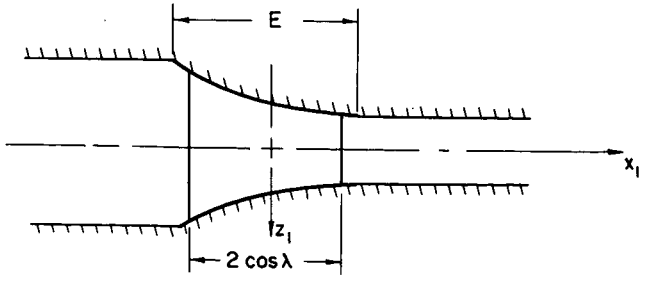


FIGURE 4$b$.—*Nondimensional contracting flow problem, with a finite length exponential channel and airfoils of chord length* $c=2$.

Hence, for the special geometry chosen, the contraction parameter $\alpha$ is related to the axial velocity ratio by the formula

$$\alpha=\frac{1}{2\cos\lambda}\ln(\mathrm{AVR}) \tag{9}$$

## Airfoil Sections

The principal geometrical features of any airfoil section are the camber line function $y_c(x)$ and the thickness distribution $y_{th}(x)$.

From figure 2 we see that the camber angle $\theta$ is a convenient index for describing the camber line. This is especially true of a symmetrically cambered foil for which $\theta/2$ measured at the leading edge is identical with $\theta/2$ measured at the trailing edge. Now, for design purposes it is often useful to be able to prescribe the section lift coefficient $C_b$ of an isolated airfoil in terms of the camber angle. Two simple camber line functions are of special practical interest: the parabolic arc and the circular arc. They are shown schematically in figure 5, indicating how the camber angle $\theta$ is measured for each one. From thin airfoil theory, the section lift coefficient due to camber for the *parabolic* arc is (ref. 6)

$$C_b=\pi\tan\frac{\theta}{2}\doteq\pi\frac{\theta}{2}\left(1+\frac{1}{12}\theta^2+\cdots\right) \tag{10}$$

Using the Joukowski transformation, the section lift coefficient for a circular arc camber line at an angle of attack $\alpha^*$ is (ref. 6, p. 69)

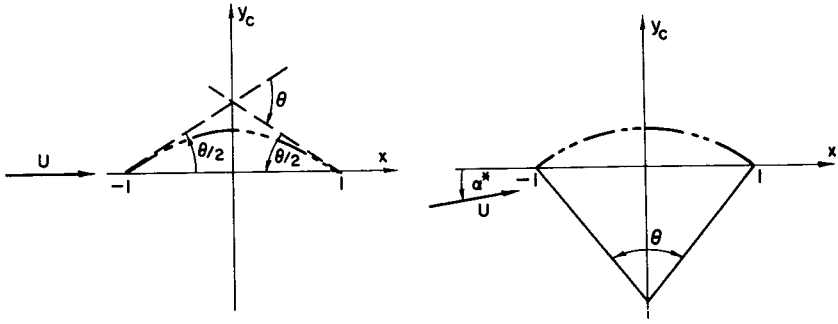


Parabolic Arc Camberline

$$\frac{dy_c}{dx}=A_1x$$

where: $A_1=-\frac{C_b}{\pi}$

Circular Arc Camberline

$$\frac{dy_c}{dx}=-\frac{x}{\sqrt{\csc^2\frac{\theta}{2}-x^2}}$$

where: $\theta=\theta(C_b)$

FIGURE 5.—*Parabolic and circular-arc camber lines.*

$$C_b = 2\pi \frac{\sin(\alpha^* + \theta/4)}{\cos \theta/4} \tag{11}$$

Putting $\alpha^* = 0$, the lift coefficient due to camber for a *circular* arc is

$$C_b = 2\pi \tan \frac{\theta}{4} \doteq \frac{\pi\theta}{2}\left(1 + \frac{1}{48}\theta^2 + \cdots\right) \tag{12}$$

Clearly, for reasonably small camber angles, $\theta$, these lift coefficients are nearly the same.

It is convenient to prescribe the camber-line slope in terms of a polynomial

$$\frac{dy_c}{dx} = A_0 + A_1 x + A_2 x^2 \tag{13}$$

The present calculations use a parabolic symmetric camber line with $C_b(\theta)$ from equation (10), so that in equation (13)

$$\left.\begin{aligned} A_0 &= A_2 = 0 \\ A_1 &= -\frac{C_b}{\pi} \end{aligned}\right\} \tag{14}$$

and

$$\theta = 2 \tan^{-1} \frac{C_b}{\pi} \qquad \text{(parabolic arc)} \tag{15}$$

A circular arc camber line could be only *approximately* represented by equation (13). The camber angle $\theta$, given $C_b$, is determined from

$$\theta = 4 \tan^{-1} \frac{C_b}{2\pi} \qquad \text{(circular arc)} \tag{16}$$

The present computations were performed using a thickness distribution $y_{th}(x)$ of a symmetrical Joukowski airfoil. The thickness slope is

$$\frac{dy_{th}}{dx} = (0.77)\frac{t}{c}\left(\tan \frac{\varphi}{2} - 2 \sin \varphi\right) \tag{17}$$

where $x = \cos \varphi$.

One of the direct results of the QTD analysis is the determination of the coefficients in the thin airfoil vorticity series

$$\gamma(x) = a_0 \tan \frac{\varphi}{2} + \sum_{n=1}^{N} a_n \sin(n\varphi) \tag{18}$$

For purposes of the calculations, the number of terms $N$ in this series was limited to 5. This is used throughout. However, a higher number of terms might be better, especially for the larger values of the stagger angle $\lambda$ and for the larger solidities $\sigma$.

The total circulation (measured positive counterclockwise; see fig. 1*b*) for both the two-dimensional and three-dimensional calculations is given by

$$\Gamma_t = \pi\left(a_0 + \frac{a_1}{2}\right) \tag{19}$$

For the two-dimensional cascades, a lift coefficient can be calculated directly from the circulation. Correcting for the sign of $\Gamma_t$ from equation (19), the lift per unit span is

$$L = -\rho V_m \Gamma_t$$

Then

$$C_L = \frac{L}{\frac{1}{2}\rho V_m^2 c} = -\frac{\Gamma_t}{\frac{1}{2}V_m c}$$

This is nondimensionalized using $c=2$ and $V_m=1$. Hence the lift coefficient for an airfoil in the two-dimensional cascade system is

$$C_L = -\Gamma_t \tag{20}$$

### Values Used in Present Computations

The results presented in this note have been calculated for a range of stagger angles and solidities with a thickness ratio of 0 and 0.1 and for mean angles of attack of 0 and 0.1 radians. The camber parameter $C_b$ was taken to be unity and the contraction parameter $\alpha$ was taken to be 0 (two-dimensional) and 0.1. The extent of the contraction was always 1.1 times the axial projection of the blade. It was found sufficient to use five terms in the vorticity series. The resulting calculations required a 15-second execution time (per each solidity and stagger angle combination) for the two-dimensional case and 48 seconds for the quasi-three-dimensional case on the IBM 7094 computer.

## RESULTS: EFFECT OF FLOW ACCELERATION ON FLOW TURNING

In this section, the main results of this note are presented in the form of nondimensional plots of the deviation angle. As mentioned previously, the calculations were performed assuming parabolically cambered airfoils with a prescribed section lift coefficient $C_b$. Computations illustrating the

effect of foil thickness ($t/c$) are presented only for $\sigma = 1$, using the symmetrical Joukowski thickness distribution discussed earlier.

Throughout the ensuing discussion the term "flow turning" will refer to the change in the flow angle $\Delta\beta = (\theta + i) - \delta^*$. This conforms to the usual convention and is the one adopted in references 3, 4, and 5. Comparisons made between two- and three-dimensional flows assume a given inlet condition; so the incidence angle $i$ can be thought of as constant at a given $\lambda$ and $\sigma$. Hence it is actually $(-\delta^*)$ that measures changes in $\Delta\beta$.

Flow turning through a cascade with accelerating flow is influenced by two factors: the magnitude of the circulation $\Gamma_{3D}$ about the blades and the increase in axial velocity. It has been pointed out (refs. 3 and 4) that the reduced circulation caused by axial-flow acceleration weakens the ability of the cascade to turn the flow, but the speed-up in axial velocity tends to make the flow more axial, and hence acts to increase the flow turning in compressor cascades. The final balance between these effects is complicated and appears to involve all the parameters of the cascade and flow geometry.

## Zero Thickness Cascade Blades

Flow turning represented in terms of the nondimensional deviation angle $\delta^*/\theta$ can be described as a function of the stagger angle $\lambda$, the solidity $\sigma$, the particular choice of camber-line function $y_c(x)$, and the inlet flow conditions represented by $\beta_1$ (or, better, by the incidence angle $i$).

Figures 6 and 7 are graphs of the change in $\delta^*/\theta$ due to accelerated flow divided by the quantity (AVR-1), plotted two different ways for convenient use. An important feature of these graphs is that the values of $\delta^*/\theta$ appearing in the quantity $\Delta[\delta^*/\theta] = (\delta^*/\theta)(2D) - (\delta^*/\theta)(3D)$ have values of two-dimensional minimum loss incidence from Lieblein (ref. 1, Chapter VI). This was accomplished by first establishing the minimum-loss-incidence angles from figure 138 of Lieblein's report. For each of the eight stagger angles $\lambda$ (see the section on the quasi-two-dimensional cascade) and the prescribed camber angle $\theta = 35.314°$, the appropriate incidence angle $i$ appearing in $\beta_1 = \lambda + \theta/2 + i$ was determined by interpolation. The incidence angles found in this manner are referred to as $i_{ml}^{(2D)}$. From the computer results, values of $(\delta^*/\theta)(2D)$ and $(\delta^*/\theta)(3D)$ are known at two different values of the mean angle of attack $\alpha_m$ (one block of calculations at $\alpha_m = 0$ and another at $\alpha_m = 0.1$). By assuming a straight-line variation of $\delta^*/\theta$ between the two $\alpha_m$ values, the angles $i_{ml}^{(2D)}$ can be cross-plotted on the same graph to obtain $(\delta^*/\theta)(2D, i_{ml}^{(2D)})$ and $(\delta^*/\theta)(3D, i_{ml}^{(2D)})$ by interpolation. Note that this means that the plane flow $\delta^*/\theta$ is compared with the accelerated flow $\delta^*/\theta$ at the *same* inlet condition; namely, minimum loss incidence. From figures 6 and 7, it is clear that the effect of flow acceleration (AVR$>$1) is larger when the

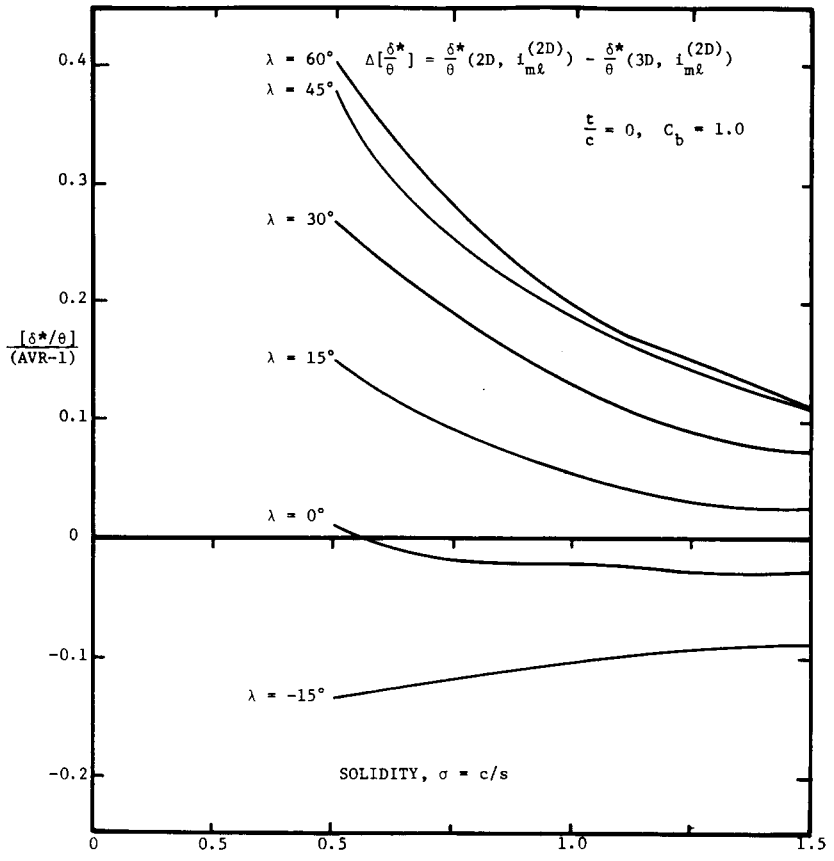


FIGURE 6.—*Effect of flow acceleration on the deviation angle ratio at minimum-loss incidence* $i_{ml}^{(2D)}$.

foils are relatively far apart ($\sigma \to 0$) and that the influence of flow acceleration is diminished as the foils are brought closer together ($\sigma$ increases). The character of the change in $\delta^*$ due to AVR$>1$ is also altered as $\lambda$ increases; i.e., $\Delta[\delta^*/\theta]$ has a steeper curve for the higher $\lambda$ values. It also changes sign for $\lambda<0$ (compare the case of $\lambda=-15°$). In the case of $\lambda=0°$, extremely small values of $\Delta[\delta^*/\theta]$ were obtained and, from a practical design point of view, it would be best to assume $\Delta[\delta^*/\theta]=0$ for $\lambda=0°$.

The mean angle of attack $\alpha_m$ is not a constant in figures 6 and 7, but varies with the appropriate minimum-loss-incidence angles $i_{ml}^{(2D)}$.

Several things should be kept in mind concerning the minimum-loss-incidence angles $i_{ml}^{(2D)}$: (1) they were determined experimentally by finding the minimum points on the curves of total pressure loss coefficient

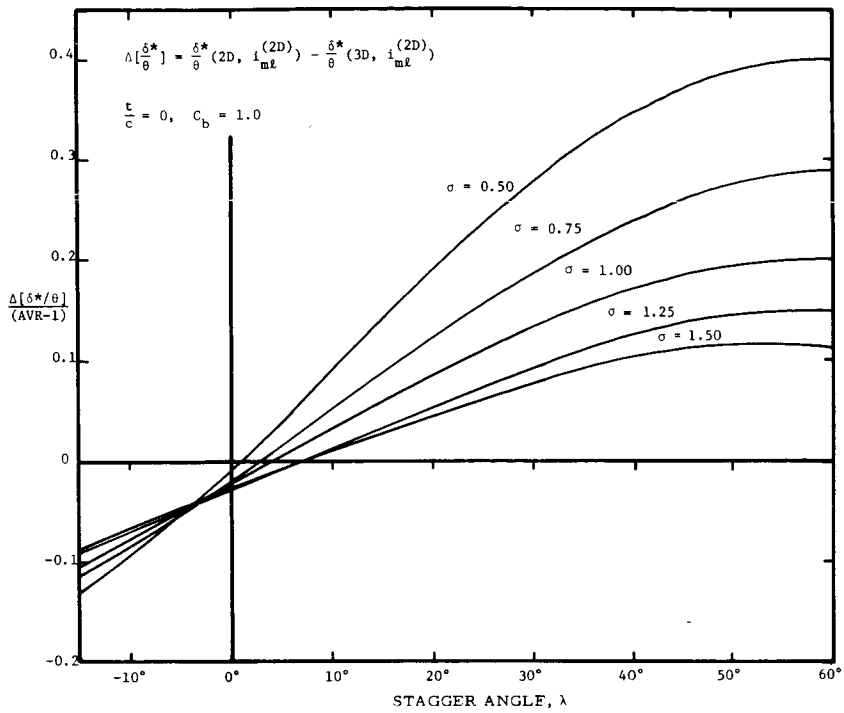


FIGURE 7.—*Effect of flow acceleration on the deviation angle ratio at minimum-loss incidence* $i_{ml}^{(2D)}$.

versus incidence angle $i$ and (2) the experiments that formed the basis for figure 138 of Lieblein's work were performed with NACA 65-($A_{10}$)-series airfoils, and the results were referred to equivalent circular-arc camber lines.

The impact-free-entry operation of an airfoil is a useful reference condition in design. Large velocity peaks on either foil surface of zero thickness blades are avoided by locating the forward stagnation point exactly at the leading edge. This simple impact-free criterion is not applicable to nonzero-thickness blades with rounded leading edges, but it seems reasonable to apply it to zero-thickness airfoils in a cascade. This was first done by Weining in his approximate theory of a two-dimensional cascade of cambered airfoils (see ref. 1, Chapter VI). For thin airfoil theory, impact-free entry corresponds to arranging the inlet flow angle $\beta_1$ so that the coefficient $a_0$ equals zero in the vorticity series (eq. (18)). The incidence angle $i$ leading to the condition $a_0=0$ can be referred to as an impact-free incidence, $i_{a_0}=0$. Values of this parameter for two-dimensional cases using the present theory were determined by interpolation. Figure 8 is a plot comparing the experimental values of

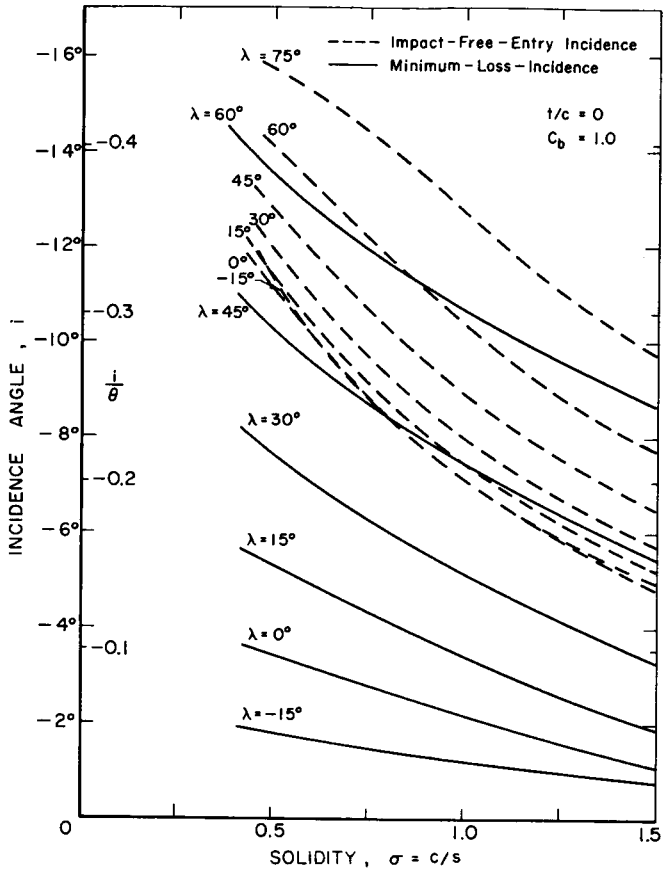


FIGURE 8.—*Comparison between experimental minimum-loss-incidence angles (Lieblein, ref. 1) and potential theory impact-free incidence.*

impact-free incidence $i_{a_0}{}^{(2D)}=0$ using the QTD theory with $\alpha=0$. Both are for zero-thickness airfoils. The two sets of curves are seen to agree only somewhat at high values of $\lambda$, and disagree completely for the lower and minus values of $\lambda$. It is for this reason that we chose inlet conditions corresponding to values of the experimental minimum-loss incidence $i_{ml}^{(2D)}$ in presenting the curves of $\Delta[\delta^*/\theta]$ in figures 6 and 7.

## Mutual Influence of Thickness Ratio and Flow Acceleration

To study the effects of thickness, a limited number of computations were carried out for a 0.1-thickness-ratio cascade of parabolic-arc camber-line airfoils of unit solidity and a camber of 35.314°. A range of stagger angles from −15° to 75° was considered. The mean angle of attack was

assumed to be zero. Both quasi-two-dimensional and plane flows were considered, with $\alpha = 0.1$ and $E = 2.2 \cos \lambda$ for the quasi-two-dimensional flows. Thickness, in general, tends to increase deviation angles. In table III of the appendix, we present values of the parameter $\delta^*/\theta(t/c=0) - \delta^*/\theta(t/c=0.1)$ for both plane and quasi-two-dimensional flows. The table shows that, in quantitative terms, the effect of thickness in increasing deviation angles is practically identical for plane and QTD flows. Based on these results, it seems reasonable to suggest that the results of figures 6 and 7 will be directly and quantitatively applicable to finite-thickness-ratio cascades as well.

## SUMMARY

Flow turning is an important aspect in the design of a compressor row, and it is known that changes in axial-flow velocity through the row can modify cascade performance. In this note, figures 6 through 8 summarize some results concerning the effects on the deviation angle of both axial-flow acceleration and changes in foil thickness. These curves are presented in a fashion that should be useful for design purposes.

The curves of $\Delta[\delta^*/\theta]/(\text{AVR-1})$ versus $\sigma$ and $\lambda$ in figures 6 and 7 combine both experimental and theoretical results. Two-dimensional experimental values of minimum-loss-incidence angles from Lieblein were cross-plotted with potential flow results for $\delta^*/\theta$ from the QTD theory in order to generate values for these graphs. In these two figures, the mean angle of attack $\alpha_m$ is not constant but varies with both $\lambda$ and $\sigma$.

All of the results presented here pertaining to the effects of axial velocity ratio on cascade performance are valid for small contraction parameter $\alpha = \ln (\text{AVR})/2 \cos \lambda$. Whatever trends are evident can be thought of as being linear in terms of this parameter, since the present QTD calculation is essentially a regular perturbation expansion in $\alpha$. This fact is useful in extrapolating the present results to other small values of the contraction parameter.

We should emphasize that the effects displayed in the graphs of this report are to be taken as trends since they actually apply to a finite exponential contraction and not necessarily to an actual contraction. Also, we have not made a systematic exhaustive numerical study of all the variables at our disposal. For example, variations in the extent of contraction, the camber angle, and the camber-line function are not considered here. However, before further calculations of this type are undertaken, it would be very desirable to have experimental results available from cascade experiments in which the contraction effect and flow geometry are well defined.

## LIST OF SYMBOLS

| | |
|---|---|
| AVR | Axial velocity ratio $= Va_2/Va_1$ |
| $A_0, A_1, A_2$ | Coefficients of the camber line slope (eq. 13)) |
| $a_0, a_1, \ldots, a_N$ | Coefficients of the vorticity series (eq. (18)) |
| $C_b$ | Section lift coefficient due to camber |
| $c$ | Chord length of airfoil |
| $E$ | Extent of cascade blades along the $x_1$ direction (fig. 4*b*) |
| $h$ | Width function of channel $= h(x_1)$ |
| $i$ | Incidence angle (see fig. 2) |
| $i_{a_0=0}^{(2D)}, i_{a_0=0}^{(3D)}$ | Incidence angles for impact-free entry (for $t/c=0$), for two-dimensional and three-dimensional cascades, respectively |
| $i_{ml}^{(2D)}$ | Incidence angle of minimum-loss operation (2D cascade) |
| QTD | Quasi-two-dimensional; refers to the spanwise averaged three-dimensional flow developed in reference 3 |
| $s$ | Spacing between foils in a cascade (see fig. 2) |
| $t/c$ | Thickness/chord ratio |
| $Va_1, Va_2$ | Axial flow velocity components at the leading edge and trailing edge, respectively |
| $V_1, V_2$ | Total velocity at the leading edge and trailing edge, respectively |
| $V_m$ | Mean total velocity, $\frac{1}{2}(V_1+V_2)$ |
| $x, y, z$ | Coordinate system with $x_1$ taken along the axial direction (cascade axis) |
| 2D | Refers to plane flow cascades, $h(x_1) =$ constant |
| 3D | Refers to three-dimensional (QTD) cascades; for the present calculations, a constant contraction parameter $\alpha = 0.1$ was used |
| $\alpha$ | Contraction parameter, exp $(2\alpha \cos \lambda)$ |
| $\alpha_m$ | Mean angle of attack of $V_m$ (see fig. 2) |
| $\alpha_m^{(2D)}, \alpha_m^{(3D)}$ | Mean angle of attack corresponding to minimum-loss incidence for two-dimensional and three-dimensional cascades, respectively |
| $\alpha_{m_{a_0=0}}^{(2D)}, \alpha_{m_{a_0=0}}^{(3D)}$ | Mean angle of attack corresponding to impact-free entry for two-dimensional and three-dimensional cascades, respectively |
| $\beta_m$ | Mean flow angle, $\lambda+\alpha_m$ |
| $\beta_1, \beta_2$ | Inlet and outlet flow angles, measured with respect to the cascade axis |
| $\gamma(x)$ | Vorticity distribution (eq. (18)) |
| $\Gamma_t$ | Total circulation (positive counterclockwise); we also use $\Gamma = -\Gamma_t$ for parts of the discussion |

| | |
|---|---|
| $\Delta[\delta^*/\theta]$ | Change in $\delta^*/\theta$ due to axial-flow acceleration, $\delta^*/\theta(2D)-\delta^*/\theta(3D)$ |
| $\Delta_{t/c}^{(2D)}[\delta^*/\theta]$ | Change in $\delta^*/\theta$ due to thickness change for two-dimensional cascade, $\delta^*/\theta(t/c=0)-\delta^*/\theta(t/c=.1)$ |
| $\Delta_{t/c}^{(3D)}[\delta^*/\theta]$ | Same as above for three-dimensional cascade |
| $\delta^*$ | Deviation angle (see fig. 2) |
| $\lambda$ | Stagger angle, angle of foil chord with axial direction |
| $\sigma$ | Solidity, $c/s$ |
| $\theta$ | Camber angle, $\frac{1}{2}(\theta_1+\theta_2)$ (see fig. 2) |

TABLE I.—*Flow Characteristics of Cascades With Parabolic Camber-Line Zero-Thickness Airfoils at Zero Mean Angle of Attack*

| Two-dimensional cascades ($\alpha=0$) | | | | | | Quasi two-dimensional cascades ($\alpha=0.1$) | | | |
|---|---|---|---|---|---|---|---|---|---|
| Stagger angle | Solidity | Incidence angle | Deviation angle | Deviation angle ratio | —Total circulation | Incidence angle | Deviation angle | Deviation angle ratio | —Total circulation |
| $\lambda$(deg) | $\sigma=\frac{c}{s}$ | $i$ (deg) | $\delta^*$ (deg) | $\delta^*/\theta$ | $\Gamma=-\Gamma_t$ | $i$ (deg) | $\delta^*$ (deg) | $\delta^*/\theta$ | $\Gamma=-\Gamma_t$ |
| −15 | 0.5 | −11.03 | 11.42 | .323 | .933 | −12.43 | 12.29 | 0.348 | 0.970 |
| | 0.75 | − 8.38 | 9.11 | .258 | .864 | − 9.75 | 9.88 | 0.280 | 0.896 |
| | 1.0 | − 6.31 | 7.39 | .209 | .788 | − 7.66 | 8.07 | 0.229 | 0.816 |
| | 1.25 | − 4.75 | 6.12 | .173 | .715 | − 6.07 | 6.73 | 0.191 | 0.740 |
| | 1.5 | − 3.57 | 5.19 | .147 | .649 | − 4.85 | 5.74 | 0.163 | 0.672 |
| 0 | 0.5 | −11.16 | 11.16 | .316 | .911 | −11.38 | 11.26 | 0.319 | 0.888 |
| | 0.75 | − 8.82 | 8.82 | .250 | .829 | − 9.15 | 8.98 | 0.254 | 0.806 |
| | 1.0 | − 7.1 | 7.1 | .201 | .746 | − 7.5 | 7.30 | 0.207 | 0.724 |
| | 1.25 | − 5.85 | 5.85 | .166 | .669 | − 6.29 | 6.06 | 0.172 | 0.650 |
| | 1.5 | − 4.93 | 4.93 | .140 | .602 | − 5.39 | 5.14 | 0.146 | 0.586 |
| 15 | 0.5 | −11.57 | 11.20 | .317 | .909 | −10.77 | 10.47 | 0.296 | 0.820 |
| | 0.75 | − 9.49 | 8.82 | .25 | .824 | − 8.94 | 8.30 | 0.235 | 0.742 |
| | 1.0 | − 8.0 | 7.05 | .20 | .738 | − 7.63 | 6.71 | 0.190 | 0.664 |
| | 1.25 | − 6.94 | 5.76 | .163 | .660 | − 6.69 | 5.54 | 0.157 | 0.594 |
| | 1.5 | − 6.18 | 4.83 | .137 | .592 | − 6.0 | 4.66 | 0.132 | 0.534 |

| | | | | | | | | | |
|---|---|---|---|---|---|---|---|---|---|
| 30 | 0.5 | −12.24 | 11.58 | .328 | .926 | −10.96 | 10.26 | 0.290 | 0.790 |
| | 0.75 | −10.37 | 9.13 | .258 | .850 | −9.44 | 8.13 | 0.230 | 0.723 |
| | 1.0 | − 9.04 | 7.25 | .205 | .767 | − 8.34 | 6.51 | 0.184 | 0.652 |
| | 1.25 | − 8.11 | 5.87 | .166 | .688 | − 7.58 | 5.32 | 0.151 | 0.585 |
| | 1.5 | − 7.46 | 4.87 | .138 | .618 | − 7.03 | 4.44 | 0.126 | 0.526 |
| 45 | 0.5 | −13.17 | 12.34 | .349 | .963 | −12.00 | 10.90 | 0.308 | 0.818 |
| | 0.75 | −11.50 | 9.83 | .278 | .911 | −10.66 | 8.70 | 0.246 | 0.772 |
| | 1.0 | −10.28 | 7.75 | .219 | .841 | − 9.67 | 6.88 | 0.1945 | 0.712 |
| | 1.25 | − 9.44 | 6.18 | .175 | .764 | − 8.98 | 5.51 | 0.156 | 0.647 |
| | 1.5 | − 8.87 | 5.04 | .143 | .690 | − 8.50 | 4.51 | 0.128 | 0.585 |
| 60 | 0.5 | −14.38 | 13.57 | .384 | 1.017 | −13.67 | 12.53 | 0.355 | 0.906 |
| | 0.75 | −12.97 | 11.12 | .315 | 1.02 | −12.48 | 10.26 | 0.290 | 0.905 |
| | 1.0 | −11.84 | 8.7 | .246 | .990 | −11.52 | 8.04 | 0.228 | 0.878 |
| | 1.25 | −11.05 | 6.70 | .19 | .928 | −10.83 | 6.19 | 0.1751 | 0.924 |
| | 1.5 | −10.55 | 5.28 | .15 | .848 | −10.39 | 4.88 | 0.1381 | 0.754 |
| 75 | 0.5 | −15.89 | 15.36 | .435 | 1.079 | −15.66 | 14.98 | 0.424 | 1.028 |
| | 0.75 | −14.94 | 13.45 | .381 | 1.189 | −14.79 | 13.11 | 0.372 | 1.128 |
| | 1.0 | −13.95 | 10.52 | .298 | 1.319 | −13.88 | 10.27 | 0.290 | 1.248 |
| | 1.25 | −13.22 | 7.18 | .203 | 1.352 | −13.18 | 6.99 | 0.198 | 1.285 |
| | 1.5 | −12.84 | 4.87 | .138 | 1.266 | −12.82 | 4.70 | 0.133 | 1.206 |

$t/c=0$ $c_b=1.0$

$\alpha_m=0$ $E/2\cos\lambda=1.1$ $\theta=35.314°$

TABLE II.—*Flow Characteristics of Cascades With Parabolic Camber-line Zero-Thickness Airfoils at 5.73° Mean Angle of Attack*

| | Two-dimensional cascades ($\alpha=0$) | | | | | Quasi two-dimensional cascades ($\alpha=0.1$) | | | |
|---|---|---|---|---|---|---|---|---|---|
| Stagger angle | Solidity | Incidence angle | Deviation angle | Deviation angle ratio | —Total circulation | Incidence angle | Deviation angle | Deviation angle ratio | —Total circulation |
| $\lambda$(deg) | $\sigma=\frac{c}{s}$ | $i$ (deg) | $\delta^*$ (deg) | $\delta^*/\theta$ | $\Gamma=-\Gamma_t$ | $i$ (deg) | $\delta^*$ (deg) | $\delta^*/\theta$ | $\Gamma=-\Gamma_t$ |
| −15 | 0.5 | −1.32 | 13.38 | .379 | 1.472 | −2.49 | 14.08 | 0.398 | 1.464 |
| | 0.75 | 2.44 | 10.09 | .286 | 1.328 | 1.20 | 10.77 | 0.305 | 1.319 |
| | 1.0 | 5.08 | 7.84 | .222 | 1.181 | 3.83 | 8.47 | 0.240 | 1.174 |
| | 1.25 | 6.90 | 6.33 | .179 | 1.047 | 5.66 | 6.91 | 0.196 | 1.043 |
| | 1.5 | 8.18 | 5.28 | .15 | .933 | 6.96 | 5.82 | 0.1649 | 0.931 |
| 0 | 0.5 | −2.01 | 13.12 | .371 | 1.431 | −1.99 | 13.01 | 0.368 | 1.359 |
| | 0.75 | 1.06 | 9.79 | .277 | 1.265 | 0.88 | 9.85 | 0.279 | 1.200 |
| | 1.0 | 3.09 | 7.56 | .214 | 1.108 | 2.79 | 7.71 | 0.218 | 1.051 |
| | 1.25 | 4.44 | 6.06 | .172 | .973 | 4.08 | 6.25 | 0.177 | 0.924 |
| | 1.5 | 5.36 | 5.02 | .142 | .861 | 4.98 | 5.23 | 0.148 | 0.819 |
| 15 | 0.5 | −3.00 | 13.28 | .376 | 1.428 | −2.12 | 12.35 | 0.350 | 1.292 |
| | 0.75 | −0.42 | 9.85 | .279 | 1.258 | 0.14 | 9.24 | 0.262 | 1.135 |
| | 1.0 | 1.23 | 7.53 | .213 | 1.097 | 1.58 | 7.15 | 0.202 | 0.988 |
| | 1.25 | 2.29 | 5.98 | .169 | .959 | 2.52 | 5.73 | 0.1625 | 0.864 |
| | 1.5 | 3.0 | 4.92 | .139 | .845 | 3.15 | 4.76 | 0.135 | 0.762 |

| | | | | | | | | | |
|---|---|---|---|---|---|---|---|---|---|
| 30 | 0.5 | −4.28 | 13.93 | .394 | 1.466 | −3.10 | 12.44 | 0.3530 | 1.289 |
| | 0.75 | −2.04 | 10.30 | .292 | 1.308 | −1.26 | 9.21 | 0.2610 | 1.146 |
| | 1.0 | −0.65 | 7.77 | .220 | 1.147 | −0.10 | 6.99 | 0.1980 | 1.002 |
| | 1.25 | 0.21 | 6.09 | .172 | 1.003 | 0.63 | 5.50 | 0.1560 | 1.876 |
| | 1.5 | 0.76 | 4.96 | .140 | .883 | 1.11 | 4.50 | 0.1275 | 0.771 |
| 45 | 0.5 | −5.85 | 15.20 | .430 | 1.546 | −4.90 | 13.66 | 0.387 | 1.371 |
| | 0.75 | −3.92 | 11.28 | .320 | 1.431 | −3.30 | 10.09 | 0.286 | 1.263 |
| | 1.0 | −2.71 | 8.33 | .236 | 1.279 | −2.29 | 7.43 | 0.210 | 1.126 |
| | 1.25 | −2.00 | 6.37 | .180 | 1.126 | −1.69 | 5.70 | 0.161 | 0.989 |
| | 1.5 | −1.57 | 5.10 | .144 | .991 | −1.32 | 4.56 | 0.129 | 0.871 |
| 60 | 0.5 | −7.81 | 17.35 | .491 | 1.668 | −7.22 | 16.11 | 0.456 | 1.539 |
| | 0.75 | −6.22 | 13.22 | .374 | 1.665 | −5.92 | 12.32 | 0.349 | 1.530 |
| | 1.0 | −5.17 | 9.37 | .265 | 1.564 | −4.99 | 8.68 | 0.246 | 1.433 |
| | 1.25 | −4.62 | 6.81 | .193 | 1.396 | −4.50 | 6.28 | 0.1775 | 1.278 |
| | 1.5 | −4.32 | 5.26 | .149 | 1.230 | −4.24 | 4.84 | 0.1370 | 1.126 |
| 75 | 0.5 | −10.22 | 20.70 | .586 | 1.812 | −10.1 | 20.4 | 0.576 | 1.756 |
| | 0.75 | −9.32 | 17.49 | .495 | 2.094 | −9.25 | 17.16 | 0.485 | 2.023 |
| | 1.0 | −8.54 | 11.25 | .319 | 2.304 | −8.52 | 10.98 | 0.310 | 2.219 |
| | 1.25 | −8.25 | 6.48 | .184 | 2.109 | −8.23 | 6.31 | 0.1785 | 2.031 |
| | 1.5 | −8.15 | 4.26 | .121 | 1.837 | −8.14 | 4.11 | 0.116 | 1.770 |

$t/c=0$ $c_b=1.0$

$\alpha_m=0.1\text{rad}=5.73°$ $E/2\cos\lambda=1.1$ $\theta=35.314°$

TABLE III.—*Values of Parameter* $[\delta^*/\theta\ (t/c=0)-\delta^*/\theta\ (t/c=0.1]$ *as a Function of Stagger Angle* $\lambda$ *for a Parabolic Arc Camber-Line Airfoil Cascade*[1]

| $\lambda$ degrees | Parameter for Q.T.D. flow | Parameter for T.D. flow |
|---|---|---|
| −15 | 0.000 | −0.001 |
| 0 | −0.011 | −0.012 |
| 15 | −0.025 | −0.025 |
| 30 | −0.040 | −0.041 |
| 45 | −0.0575 | −0.057 |
| 60 | −0.076 | −0.075 |
| 75 | −0.106 | −0.107 |

[1] In the quasi-two-dimensional case, $\alpha = 0.1$ and $E = 2.2 \cos \lambda$. Also, $\alpha_m = 0$, $\sigma = 1$ and $\Theta = 35.314°$ for both cases.

## REFERENCES


1. JOHNSON, I. A., AND R. O. BULLOCK, eds., *Aerodynamic Design of Axial-Flow Compressors*. NASA SP–36, 1965 (especially Chapters VI and VII).
2. MELLOR, G. L., An Analysis of Axial Compressor Cascade Aerodynamics. Part I and Errata (December 1962), *Trans. ASME, J. Basic Eng.*, Ser. D, Vol. 81, September 1959.
3. MANI, RAMANI, *Quasi Two-Dimensional Flows Through Cascades*. Ph.D. dissertation, Cal. Tech., December 1966.
4. MANI, RAMANI, AND A. J. ACOSTA, Quasi-Two-Dimensional Flows Through a Cascade. *Trans. ASME, J. Power*, Vol. 90, No. 2, April 1968.
5. MANI, RAMANI, *A Method of Calculating Quasi Two-Dimensional Flows Through Cascades*. Eng. Div., Cal. Tech., Report E–79.10, July 1967.
6. VON KARMAN, T., AND J. M. BURGERS, *Aerodynamic Theory*. Vol. II, Div. E, W. F. Durand, ed., 1934.
7. WILSON, M. B., AND A. J. ACOSTA, *A Note on the Influence of Axial Velocity Ratio on Potential Flow Cascade Performance*. Div. Eng. and Appl. Sci., Cal. Tech., Report E–79.11, January 1969.

## DISCUSSION

J. H. HORLOCK AND J. P. GOSTELOW (Cambridge University): We have followed the work of Mani and Acosta (and now Wilson) with considerable interest over the past few years since, at Liverpool and Cambridge, we have been working on the same problem of axial velocity ratio effects.

On the analytical side, two approaches to the problem have been described in the discussion of reference 4, referring to papers by Pollard and Horlock (ref. D–1), and Shaalan and Horlock (ref. D–2). Briefly, the first approach was to place strip sources across the blade pitch and solve the potential equations for the flow past thin airfoils in two dimensions. (This is somewhat similar to the approach of Smith, described in the first paper, in which he allows for the flow in the $S2$ plane in his solutions for the $S1$ plane.) The second approach made the initial assumption that meridional flow through the midspan section of the blade was on gently inclined planes, and a potential equation

$$\nabla^2\phi+\frac{h^1(x_1)}{h_1(x_1)}\frac{\partial\phi}{\partial x_1}=0$$

was derived for the flow *near the center line.* Solution of this equation was again obtained by using local sources $S=-(h^1/h)(\partial\phi/\partial x)$ varying linearly across the pitch. No allowance was made for the modification of the induced velocity due to restricted length of singularities. Essentially, the problem solved was two-dimensional, but one in which fluid was introduced uniformly at all values of $Z$ in order to increase the axial velocity.

Hawthorne (ref. D–3) has since argued that neither the Mani-Acosta-Wilson nor the Pollard-Horlock-Shaalan approach is strictly valid. If the Mani-Acosta-Wilson approach is more realistic than the Pollard-Horlock-Shaalan solution in its allowance for spanwise variation in singularity strength, then the effects of trailing, or shed, vorticity should also be included, downstream of the blades. Hawthorne has solved the problem for closely spaced blades using the type of analysis developed by Honda for shear flows (ref. D–4).

Another approach is that of Norbury (as yet unpublished) who considers the radial flow through "ring" airfoils. The bound singularities are then uniform but circular in shape, rather than infinitely long straight

lines (Pollard-Horlock-Shaalan) or lines of finite length (Mani-Acosta-Wilson).

Shaalan has recently provided a summary design manual similar to the current paper. It allows for axial velocity ratio effects and is based on reference D–2. A summary of Shaalan's calculations is given in figures D–1 and D–2 for 20° and 30° camber. We doubt the validity of the thin airfoil analysis, especially for cambers higher than 30°. Also shown is Howell's rule for deviation (ref. D–5), based on experimental cascade data. We expect this rule to be valid for $1.1 < \mathrm{AVR} < 1.2$. We have replotted these calculations in figure D–3 (at *zero* incidence, not minimum-loss incidence, which would be roughly $-5°$) for direct comparison with the Mani-Acosta-Wilson calculations.

We would commend the use of the parameter $\Delta[\delta^*/\theta]/(\mathrm{AVR}-1)$ to designers. This is a logical dimensionless group which adequately represents the observed linear dependence of deviation on camber (Howell) and of deviation on axial velocity ratio (Pollard and Gostelow, ref. D–5).

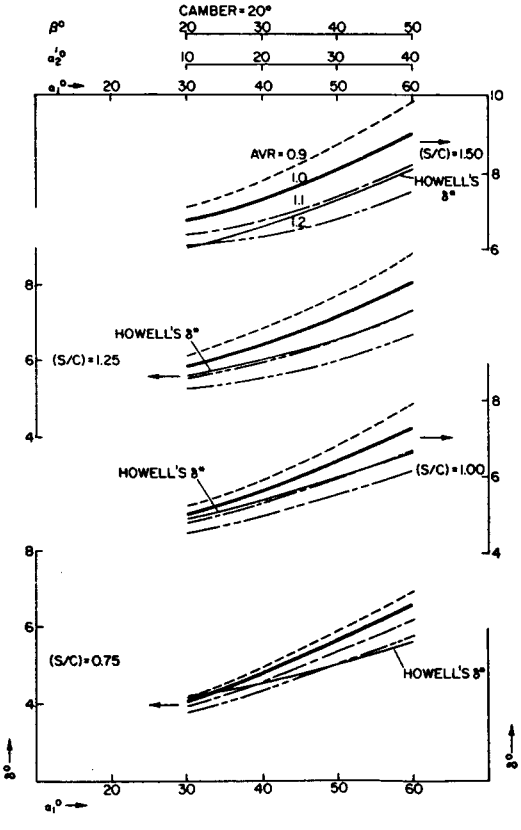


FIGURE D–1.—*Shaalan's prediction for 20° camber.*

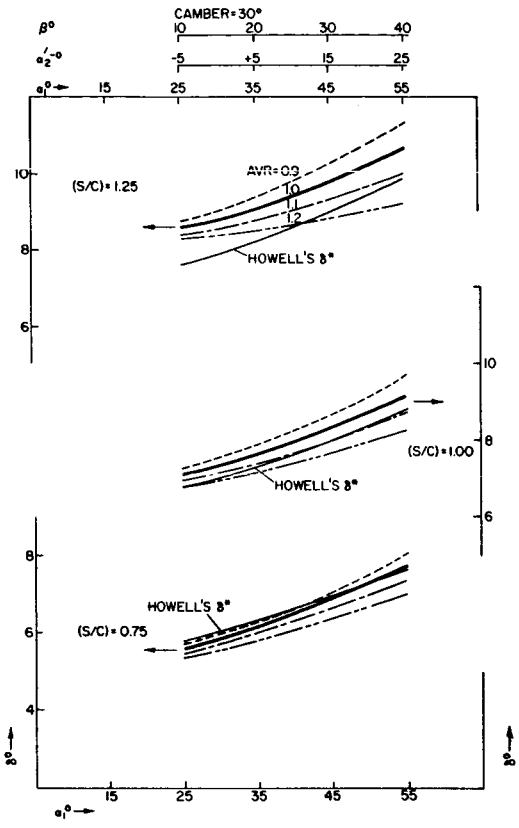


FIGURE D–2.—*Shaalan's prediction for 30° camber.*

The experimental evidence available is that of Pollard and Gostelow (ref. 13), Heilmann (ref. 14) and Masek and Norbury (ref. 15). Pollard and Gostelow used 10/C430 C50 airfoils at 36° stagger, with solidities of unity and 1.15. This resulted in the empirical rule

$$\Delta\delta^* = \delta^*_{3D} - \delta^*_{2D} = 10(\mathrm{AVR} - 1)$$

giving

$$\frac{\Delta[\delta^*/\theta]}{\mathrm{AVR}-1} = \frac{10}{30} = +0.33$$

Heilmann tested a NACA 65–(12A2 I8b)10 cascade with 25.5° stagger for minimum-loss incidence and a solidity of 1.5. The slope of the experimental results gives

$$\frac{\Delta[\delta^*/\theta]}{\mathrm{AVR}-1} = +0.15$$

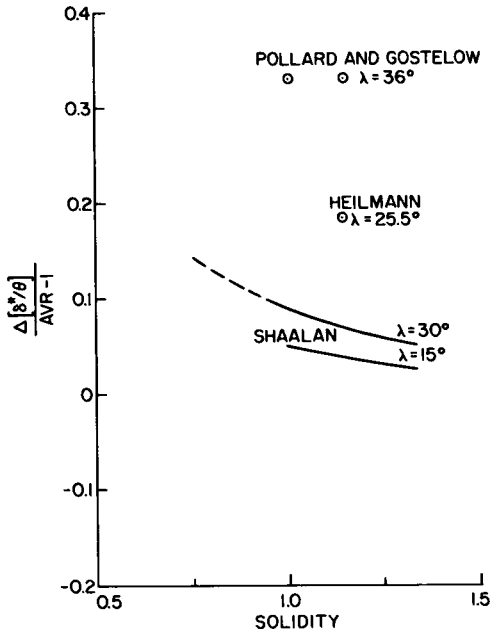


FIGURE D–3.—*Effect of axial velocity change on deviation angle ratio.*

Masek and Norbury tested a specially designed compressor cascade with 35.5° stagger and a solidity of 1.2. The slope of their experimental results, for both zero and minimum-loss incidence, gives

$$\frac{\Delta[\delta^*/\theta]}{\mathrm{AVR}-1}=+0.31$$

We understand that the thin airfoil potential theory used by Mani-Acosta-Wilson for airfoils of finite thickness neglects perturbations of chordwise velocity and of velocity gradient in the equation for source distribution. This may well result in erroneous prediction of lift and deflection. It would be of interest to see the presentation of pressure distributions from the Mani-Acosta-Wilson analysis, for comparison with Shaalan's predictions and with experimental results and for calculation of the blade boundary layers. A disadvantage of all thin airfoil theories is that the Kutta/Joukowski condition again results in erroneous prediction of lift and deflection. Real blading usually has a rounded trailing edge.

It seems that there is much more work to be done. The changes in $\Delta[\delta^*/\theta]/(\mathrm{AVR}-1)$ for off-design incidence have not been assessed either theoretically or experimentally. There may or may not be a significant change in this parameter as incidence is increased. Our own limited evidence is contradictory. The designer also needs information on the

relationship between loss coefficient and axial velocity ratio. This will need a substantial effort with both experimental work and viscous flow calculations.

B. LAKSHMINARAYANA (Pennsylvania State University): I have carried out an approximate analysis for the prediction of the change in deviation angle due to change in axial velocity through the cascade. The predicted change agrees qualitatively with those of the authors and Pollard, Horlock, and Shaalan's theory (refs. D–1 and D–2) and is in good agreement with values measured by Pollard and Gostelow (ref. D–6), Heilmann (ref. D–7), and Schulze, et al. (ref. D–9).

The change in circulation associated with change in axial velocity is given by:[D–1]

$$\Delta\Gamma = S[(V_{x_1}\tan\beta_1 - V_{x_2}\tan\beta_2') - V_{x_1}(\tan\beta_1 - \tan\beta_2)]$$

$$= SV_{x_1}(\tan\beta_2 - \mathrm{AVR}\tan\beta_2') \qquad \text{(D–1)}$$

where $\beta_2' = \beta_2 - \Delta\delta^*$ and $\beta_2$ is the outlet angle for AVR = 1.

$$\Delta\delta^* = \delta_{2d}{}^* - \delta_{3d}{}^*$$

For small values of $\Delta\delta^*$,

$$\tan\beta_2' = (\tan\beta_2 - \Delta\delta^*)(1 - \Delta\delta^*\tan\beta_2) \qquad \text{(D–2)}$$

Substituting equation (D–2) in (D–1) and neglecting the second-order term $(\Delta\delta^*)^2$,

$$\Delta\Gamma/SV_{x_1} = (1-\mathrm{AVR})\tan\beta_2 + \mathrm{AVR}\ \Delta\delta^*\sec^2\beta_2 \qquad \text{(D–3)}$$

With regard to *change in circulation* ($\Delta\Gamma$), mutual interaction of thickness and axial velocity changes should be small and this has been demonstrated by the authors (table III). Thus, the problem reduces to computation of $\Delta\Gamma$ for a cascade of cambered plates.

The circulation distribution for a cascade of symmetrically cambered (parabolic or circular) plates is given by (ref. D–10),

$$\gamma(x) = KV_m[2\alpha(1+\cos\theta)/\sin\theta + 8(G/c)\sin\theta] \qquad \text{(D–4)}$$

where

$K$ is the cascade influence coefficient (see fig. 282.1 in ref. D–10 for values)

$\alpha = i + \theta/2$

$G$ = maximum camber

$x = (c/2)(1-\cos\theta)$, the coordinate transformation

---

[D–1] All primed expressions such as $\beta_2{}^1$, $V_m{}^1$ refer to values with AVR $\neq 1$ and $V_x$ refers to axial velocities.

The change in circulation distribution due to axial velocity change (with $V_1$ and $\beta_1$ held fixed) is given by[D-2]

$$d\gamma = 2KV_m\,\Delta\alpha(1+\cos\theta)/\sin\theta + K\Delta V_m[2\alpha(1+\cos\theta)/\sin\theta + 8G/c\sin\theta] \qquad \text{(D-5)}$$

where $\Delta V_m$ for a cascade (which corresponds to the change in free-stream velocity in the case of an isolated blade) varies from zero at the leading edge to its full value at the trailing edge.

For small changes in axial velocities, the maximum change in $V_m$ can be approximated by

$$(V_m')^2 - V_m^2 \cong 2V_m(\Delta V_m)_{TE} \qquad \text{(D-6)}$$

where $V_m'$ is the vector mean velocity for a cascade with AVR$\neq 1$ and TE refers to values at the trailing edge.

Using the cascade relationships for $V_m$ and $V_m'$, equation (D-1), and the approximations indicated in equations (D-2) and (D-3), the following expression can be derived

$$\frac{(\Delta V_m)_{TE}}{V_{x1}} = \frac{1}{8}\frac{V_x}{V_m}\left\{(1+\text{AVR})^2 - 4 - \frac{\Delta\Gamma}{SV_{x1}}[(1+\text{AVR})\tan\beta_2 + 2\tan\beta_1]\right\} \qquad \text{(D-7)}$$

In equation (D-7), second-order terms such as $\Delta\delta^{*2}$ and $\Delta\Gamma\Delta\delta^*$ have been neglected.

Similarly, the trailing edge of the blade will have an incidence change (for small $\Delta\alpha_{TE}$) given by

$$\frac{\tan\beta_1'}{\tan\beta_1} = \frac{1}{\text{AVR}} = \frac{(\tan\beta_1 + \Delta\alpha_{TE})(1+\Delta\alpha_{TE}\tan\beta_1)}{\tan\beta_1}$$

Hence,

$$\Delta\alpha_{TE} = \frac{1-\text{AVR}}{\text{AVR}}\frac{\tan\beta_1}{\sec^2\beta_1} \qquad \text{(D-8)}$$

If $\Delta V_x$, $\Delta\alpha$, and $\Delta V_m$ vary linearly with $x$, it is clear that

$$\Delta\alpha = \frac{1-\text{AVR}}{2\text{AVR}}\frac{\tan\beta_1}{\sec^2\beta_1}(1-\cos\theta) \qquad \text{(D-9)}$$

---

[D-2] The analysis is based on the fact that each infinitesimally small blade element in the cascade sees a different change in angle of incidence ($\Delta\alpha$) and velocity ($\Delta V_m$) due to change in axial velocity. The values vary from zero at the leading edge to full value at the trailing edge; hence, $d\gamma$, $\Delta\alpha$, and $\Delta V_m$ are all functions of $x$ or $\theta$.

$$\Delta V_m = (\Delta V_m)_{TE} \frac{1-\cos\theta}{2} \tag{D-10}$$

Substituting equations (D–7) through (D–10) in equation (D–5) and integrating the expression between $x=0$ and $x=c$, the following expression is derived for total change in circulation

$$\frac{\Delta\Gamma}{SV_{x_1}} = \Pi K\sigma \frac{V_m}{V_{x_1}} \frac{1-\mathrm{AVR}}{4\mathrm{AVR}} \frac{\tan\beta_1}{\sec^2\beta_1} + \Pi K\sigma \left(\frac{G}{c}+\frac{\alpha}{4}\right)\left(\frac{\Delta V_m}{V_{x_1}}\right)_{TE} \tag{D-11}$$

Substituting equations (D–3) and (D–7) in (D–11) and rearranging, the following expression can be derived for the change in the deviation angle due to axial velocity change

$$\mathrm{AVR}\frac{\Delta\delta^*}{\mathrm{AVR}-1} = \cos^2\beta_2 \left\{ \tan\beta_2 + \frac{\left(\dfrac{\Pi K\sigma[(G/c)+(\alpha/4)]\cos\beta_m[(\mathrm{AVR}+1)^2-4]}{\mathrm{AVR}-1} - \dfrac{2\Pi K\sigma\tan\beta_1}{\mathrm{AVR}\cos\beta_m\sec^2\beta_1}\right)}{8+\Pi K\sigma[(\alpha/4)+(G/c)]\cos\beta_m[(\mathrm{AVR}+1)\tan\beta_2+2\tan\beta_1]} \right\} \tag{D-12}$$

Equation (D–12) provides deviation values which are better than those of either of the two theories (see discussion of this paper by Horlock and Gostelow) for the cascades of Pollard and Gostelow (ref. D–6), Heilmann (ref. D–7), and Schulze (ref. D–9) as shown in table D–I.

It is not clear why the approximate theory developed above has better agreement with experimental values than the theories developed by the authors and Pollard-Horlock-Shaalan (refs. D–1 and D–2). One possible source of error may be the numerical method. The numerical solution adopted by the authors is not capable of predicting extremely small change in angles. One way to overcome this is to solve directly for the perturbed flow, as shown in this discussion, rather than to solve for the entire cascade flow.

It should be emphasized here that all the theories, including that of the discussor, are strictly valid for small changes in AVR (possibly for $0.9<\mathrm{AVR}<1.1$) and small flow turning. At higher values of AVR and $\theta$, the three-dimensional effects are important and the flow cannot be considered quasi-two-dimensional.

TABLE D–I.—*Comparison Between Predicted and Experimental Values of* $\Delta(\delta^*/\theta)/(AVR-1)$

| Cascade | Parameters | Experimental value | Predicted | | |
|---|---|---|---|---|---|
| | | | BL | M/A/W | P/H/S (refs. D–1 and D–2) |
| Pollard and Gostelow (ref. D–6) 10/C430 C50 | $\lambda=36°$, $\sigma=1.14$ $\beta_1=52°50^1$, $\beta_2=31°$ $G/c=0.065$, $K=0.8$ $\theta=30°$, $\alpha=16°50^1$ | 0.33 | 0.42 | 0.13 | 0.09 |
| Heilmann (ref. D–7) NACA 65(12$A_2I_{8b}$)10 | $\lambda=25.5°$, $\sigma=1.5$ $\beta_1=45°$, $\beta_2=19°$ $G/c=0.073$, $K=0.65$ $\theta=31°$, $\alpha=19°30^1$ | 0.15 | 0.18 | 0.062 | 0.04 |
| Schulze, et al. (ref. D–9) NACA 65(11)10 | $\lambda=40.5°$, $\sigma=1.00$ $\beta_1=52°30^1$, $\beta_2=35°$ $G/c=0.06$, $K=0.87$ $\theta=28°$, $\alpha=12°$ | 0.37 | 0.49 | 0.175 | |

WILSON, MANI, AND ACOSTA (authors): In view of the spirited discussion of our paper at the symposium, a thorough review was carried out of all aspects of the calculations. As a result, a rather subtle but important error has been uncovered in our procedure of evaluating deviation and incidence angles once the circulation has been determined. We regret this error[D–3] deeply but, as this closure demonstrates, once this error is rectified, our results for deviation angles are in much better agreement with those of other investigators.

Having obtained the total circulation $\Gamma$ around each airfoil, we assumed previously that the row of infinite vortices would contribute tangential velocities $\pm\Gamma/2s$ on the downstream/upstream side, where $s$ is the transverse spacing between adjacent airfoils. This result is indeed

[D–3] These corrections have been incorporated in the final version of the paper published in these symposium proceedings.

true in the two-dimensional problem. It has turned out to be erroneous to $0(\alpha)$ in the quasi-two-dimensional problem. We have calculated anew these tangential velocities by summing the fundamental solution $v_v$ spelled out in Appendix 1 of reference 4 of our paper. The correct result was found to be that the tangential velocity (due to the vortices) downstream is

$$\frac{-\Gamma}{2s}\left(1+\frac{\alpha}{2}E\right)$$

where $\alpha$ is the contraction parameter and $E$ is the extent of contraction. The tangential velocity due to the vortices upstream is

$$\frac{\Gamma}{2s}\left(1-\frac{\alpha}{2}E\right)$$

Note that the difference of these tangential velocity contributions is still $\Gamma/s$ (as it should be), but the contraction introduces an asymmetry whereby the downstream contribution is enhanced by a factor $1+(\alpha/2)E$ and the upstream contribution is reduced by a factor of $1-(\alpha/2)E$. We thereby calculate the inlet flow angle with the equation

$$\tan\beta_1=\frac{\sin(\lambda+\alpha_m)+\frac{1}{2}\Delta V_t[1-(\alpha/2)E]}{(1-\alpha\cos\lambda)\cos(\lambda+\alpha_m)}$$

and the outlet flow angle by

$$\tan\beta_2=\frac{\sin(\lambda+\alpha_m)-\frac{1}{2}\Delta V_t[1+(\alpha/2)E]}{(1+\alpha\cos\lambda)\cos(\lambda+\alpha_m)}$$

where $\Delta V_t$ is still $\Gamma/s$.

As can be readily appreciated, correction of this error has the effect of decreasing (at fixed mean angle of attack) both incidence and deviation angles. Two sets of computations were performed with the corrected equations to demonstrate the vastly improved agreement of our results with those of other investigators.

First, in figure D–4, we plot the $\delta^*-i$ curves for a zero-thickness, parabolic camber line cascade with $\lambda=45°$, $\sigma=1.25$, $\theta=35.314°$, $E/2\cos\lambda=1.1$, and $\alpha=0.1$. Dr. L. H. Smith of General Electric Company, Cincinnati, Ohio, referred our paper originally to his colleague, Dr. D. C. Prince, Jr. Dr. Prince performed computations based on a finite difference method and kindly supplied us with results for the effect of the contraction on the $\delta^*-i$ curves, based on his program. Dr. Prince was among the first to express strong reservations about our results, indicating that the deviation angles may sometimes increase (due to speeding of the flow). The figure is largely self-explanatory, and it is seen that our corrected

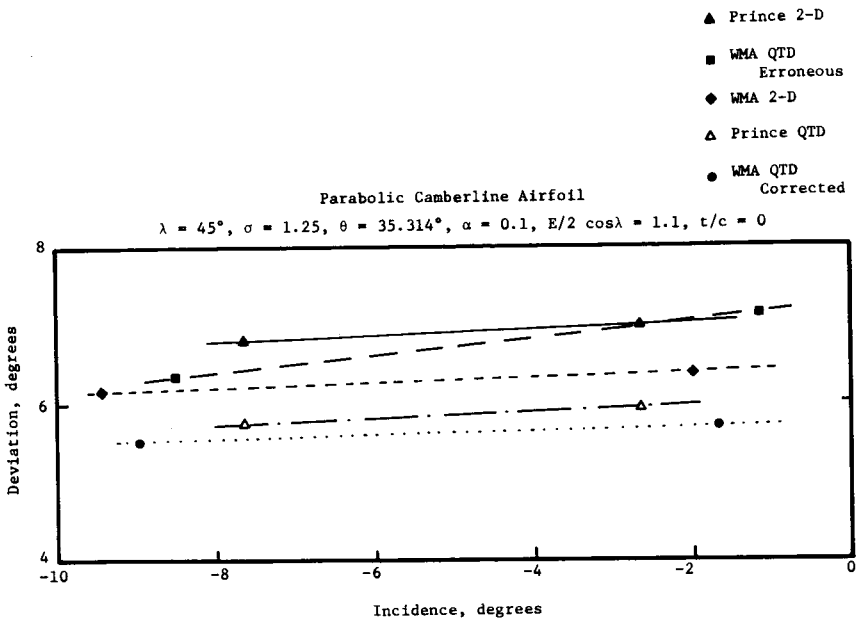


FIGURE D–4.—*Deviation angles for parabolic camber airfoil.*

results are in much better agreement with those of Dr. Prince. Our analysis predicts a drop of around 0.7° due to axial acceleration, while Dr. Prince's estimates are closer to 1° to 1.1°.

The second set of computations pertains to calculations carried out by Professor Lakshminarayana in his discussion of the paper. He considers two cases: first, a cascade with $\lambda = 36°$ and $\sigma = 1.14$ and, second, a cascade with $\lambda = 25.5°$ and $\sigma = 1.5$. By interpolation from our new (corrected) figure 7, the following results were obtained:

The table follows the notation of Professor Lakshminarayana's discussion.

It is seen that the agreement with Professor Horlock's results is now much better. A discrepancy of even 0.04 in the value of the predicted parameter with $\theta = 35°$ and AVR = 1.15 corresponds to a discrepancy in $\Delta\delta^*$ itself of only 0.21°. Considering that these results have been derived by interpolation, the agreement seems satisfactory. Professor Lakshminarayana's predictive procedure, of course, would appear to fit the experimental data the best of all. Perhaps most important, corrected results of the present paper seem to fall in line with those of other investigators in that deviation angles would appear to be always reduced due to axial acceleration for decelerating ($\lambda > 0$) cascades.

It is worth emphasizing that, in all these corrected calculations, the value of $\Gamma$ used was the same as obtained previously. No errors were

TABLE D-II.—*Comparison Between Predicted and Experimental Values of* $\Delta(\delta^*/\theta)/(AVR-1)$

| Cascade | Experimental value | Predicted | | | |
|---|---|---|---|---|---|
| | | BL | WMA, old, erroneous | WMA, new, corrected | P/H/S |
| Pollard and Gostelow | 0.33 | 0.39 | −0.05 | 0.13 | 0.09 |
| Heilmann | 0.15 | 0.16 | −0.13 | 0.062 | 0.04 |

found in the basic theory itself; namely, in the singular solutions or the setting up and solving of the integral equation.

*All graphs, tables, equations, and conclusions presented in this final version of this paper have been corrected from the earlier version.*

In conclusion, we wish to express our sincerest gratitude to several individuals, notably Drs. L. H. Smith and D. C. Prince, Jr., and Professors Horlock and Lakshminarayana, for their sustained interest in our work.

## REFERENCES

D-1. POLLARD, D., AND J. H. HORLOCK, *A Theoretical Investigation of the Effect of Change in Axial Velocity on the Potential Flow Through a Cascade of Aerofoils.* A.R.C. CP 619, 1963.

D-2. SHAALAN, M. R. A., AND J. H. HORLOCK, *The Effect of Change in Axial Velocity on the Potential Flow in Cascades.* A.R.C. R and M 3547, 1968.

D-3. HAWTHORNE, SIR WILLIAM, private communication.

D-4. HONDA, M., Theory of Shear Flow Through a Cascade. *Proc. Roy. Soc. (London)*, Ser. A, Vol. 265, 1961, pp. 46–70.

D-5. HOWELL, A. R., *The Present Basis of Axial Flow Compressor Design: Part I, Cascade Theory and Performance.* A.R.C. R and M 2095, 1942.

D-6. POLLARD, D., AND J. P. GOSTELOW, Some Experiments at Low Speed on Compressor Cascades. *Trans. ASME, J. Eng. Power*, Vol. 427, July 1967.

D-7. HEILMANN, W., Experimentelle und grenzschichttheoretische Untersuchungen an ebenen Verzögerungsgittern bei kompressibler Strömung, insbesondere bei Anderung des axialen Stromdichteverhältnisses und der Zuströmturbulenz. D.V.C. Forschungsbericht 67–88, 1967.

D-8. MAREK, Z., AND J. F. NORBURY, The Effect of Axial Velocity Variation on the Performance of a Compressor Cascade. Unpublished report, Liverpool U., 1968.

D-9. SCHULZE, W. M., et al., NACA TN 4130, October 1957.

D-10. SCHOLZ, N., *Aerodynamik der Schaufelgitter.* Band I, Verlag G. Braun, p. 165.